Soft Matter

All-atom Molecular Dynamics Simulations of Weak Polyionic Brushes: Influence of Charge Density on the Properties of Polyelectrolyte Chains, Brush-Supported Counterions, and Water Molecules

Journal:	*Soft Matter*
Manuscript ID	SM-ART-05-2020-001000.R1
Article Type:	Paper
Date Submitted by the Author:	12-Jul-2020
Complete List of Authors:	Sachar, Harnoor; University of Maryland, College Park, Mechanical Engineering Pial, Turash; University of Maryland, College Park, Mechanical Engineering Chava, Bhargav; University of Maryland, College Park, Mechanical Engineering Das, Siddhartha; University of Maryland, College Park, Mechanical Engineering

All-atom Molecular Dynamics Simulations of Weak Polyionic Brushes: Influence of Charge Density on the Properties of Polyelectrolyte Chains, Brush-Supported Counterions, and Water Molecules

Harnoor Singh Sachar,[1] Turash Haque Pial,[1] Bhargav Sai Chava,[1] and Siddhartha Das[1*]

[1]Department of Mechanical Engineering, University of Maryland,

4298 Campus Drive, College Park, MD 20742

*Email: sidd@umd.edu

ABSTRACT

All atom Molecular Dynamics (MD) simulations of planar Na^+-counterion-neutralized Polyacrylic Acid (PAA) brushes are performed for varying degrees of ionization (and thereby varying charge density) and varying grafting density. Variation in the PE charge density (or degree of ionization) and grafting density leads to massive changes of the properties of the PE molecules (quantified by the changes in the height and the mobility of the PE brushes) as well as the local arrangement and distribution of the brush-supported counterions and water molecules within the brushes. The effect on the counterions is manifested by the corresponding variation of the counterion mobility, counterion concentration, extent of counterion binding to the charged site of the PE brushes, water-in-salt-like structure formation, and counterion-water-oxygen radial distribution function within the PE brushes. On the other hand, the effect on water molecules is manifested by the corresponding variation of water-oxygen-water-oxygen RDF, local water density, water-water and water-PE functional group hydrogen bond networks, static dielectric constant of water molecules, orientational tetrahedral order parameter, and water mobility. Enforcing such varying degree of ionization of weak polyelectrolytes is possible by changing the pH of the surrounding medium. Thus, our results provide insights into the changes in microstructure (at the atomistic level) of weak polyionic brushes at varying pH. We anticipate that this knowledge will prove to be vital for the efficient design of several nano-scale systems employing PE brushes such as nanomechanical gates, current rectifiers, etc.

INTRODUCTION

Charge bearing polymer molecules or polyelectrolytes (or PEs) are undoubtedly one of the pillars of modern-day material science due to their widespread use in day-to-day life. PEs are used for synthesizing a variety of materials ranging from gels[1-3] to solutions[4-6] to blends[7-9]. One of the most intriguing architectures involving PEs is the "brush-like" form, where one end of the individual PE chain is grafted to a substrate. When grafted in close proximity to each other in a good solvent, the PE chains tend to stretch in the direction perpendicular to the substrate in order to avoid monomer-monomer contacts and reduce electrostatic repulsion between the charged segments and in the process attain such "brush-like" configuration. PE brushes find use in a multitude of applications such as nanofluidic energy conversion[10,11], biosensing[12-13], colloidal stabilization[14], oil recovery[15], drug delivery[16-17], etc. This has inspired several theoretical[18-27], computational[28-37] as well as experimental[38-47] studies to probe the structure and configuration of PE brushes.

One of the most exciting prospects about PE brushes is their ability to respond to changes in the surrounding medium like solvent quality, pH, salt concentration, etc. This structural transition of the brushes in response to their environment renders a sense of "smartness" to PE brush grafted interfaces, and forms the basis for several applications such as nanomechanical gates[48], current rectifiers[49-50], etc. One key reason for the responsiveness of weak polyanionic or polycationic PE brushes is a change in the degree of ionization of the titration sites. This is typically induced by variation in the pH of the surrounding medium, shifting the equilibrium of the acid-base reaction responsible for charging of the PE chains. Several studies have investigated the effects of changes in degree of ionization (and thereby the charge density) of PEs in solution[51-55] as well as PE brushes[56-59]. However, most of these studies have focused on the overall structural changes (macrostructure) of the PE molecules rather than the changes

occurring at the atomistic length scales (microstructure). Recently, we published the first molecular dynamics (MD) simulation study probing the local arrangement of counterions and water molecules within the planar PE brushes using an all-atom framework[60]. In the current manuscript, we take a similar approach to probe the changes in the microstructure of densely grafted Polyacrylic acid (PAA) brushes *with varying degree of ionization*. The charges on the brushes are neutralized by adding an appropriate number of Na^+ counterions to the system (depending on the degree of ionization). A 3-site SPC/E model[61] is used to explicitly resolve the water molecules. Analysis of the microstructure of the brushes is anticipated to provide us fundamental insights into their behavior and thereby envision new applications of PE brushes in the fields of nanotechnology and tribology.

Our paper is organized in the following sections. We begin with a detailed description of our MD simulation setup. Subsequently, we present our results for the brush height and chain mobility, followed by the local arrangement and distribution of the counterions and water molecules respectively. The effect on the counterions is investigated by quantifying the brush-induced changes in counterion concentration, condensation, solvation structure (and the resultant propensity to form water-in-salt like structure[60]), radial distribution function (RDF), and mobility. On the other hand, the effect on the water molecules is identified by probing the corresponding brush-induced changes in the water-oxygen-water-oxygen RDF, water-water and water-PE functional group hydrogen bond networks, water mass density, static dielectric constant, orientational tetrahedral order parameter[62], and mobility. The results demonstrate massive impact of the changes of the degree of ionization as well as the grafting density. Given that such variation in the degree of ionization can be brought about by the corresponding changes in the pH of the surrounding medium, the findings shed light to the possible impact of the pH-

responsiveness of densely grafted brushes on its properties as well as the properties and distributions of the brush-supported counterions and water molecules in an unprecedented atomistically resolved fashion. In section S1 of the Supporting Information (SI), we provide a relationship between the pH and degree of ionization of the PAA brushes.

SIMULATION DETAILS

MD simulations were conducted using an all-atom framework. We considered 36 Polyacrylic acid (PAA) chains having N=49 backbone Carbon atoms. Each chain was end-grafted on a 6 X 6 square lattice by fixing one of their terminal Carbons in the x-y plane (z=0). Each chain consisted of 24 functional groups that could exist either in the protonated state (COOH) or the deprotonated state (COO^-). The degree of ionization of the brushes f (ratio of deprotonated functional groups to total number of functional groups) was varied from no charge (f=0) to completely ionized (f=1) in steps of 0.25 i.e. f=0, 0.25, 0.5, 0.75, 1. For a given degree of ionization, 24*f functional groups were randomly ionized along the length of each chain. An equal number of Na^+ counterions were added in the simulation box to ensure charge neutrality (see Figure 1 for a snapshot of the brushes and counterions). No external salt was added to the system (salt-free brushes). 3-site SPC/E water molecules[61] were used as the explicit solvent. Two different values of brush grafting densities σ_g = $0.1/\sigma^2$ and $0.2/\sigma^2$ (where σ=3.5 Å is the LJ distance parameter for backbone Carbon atoms) were probed. Enough water molecules were added to ensure that the simulation box height was always greater than or equal to 1.5Nσ to eliminate finite size effects. Continuous LJ and reflective walls were placed at the bottom and top of the simulation box respectively to prevent counterions and water molecules from leaving the system. All simulations were performed on the MD platform LAMMPS[63] (Large-scale Atomic/Molecular Massively Parallel Simulator).

We used the OPLS-AA force field[64] to model the brushes. All bonded (bonds, angles, dihedrals, impropers) and non-bonded parameters (charge, LJ diameter, LJ well-depth) were taken from the OPLS database and provided in section S2 of the Supporting Information. A shifted truncated 12-6 Lennard Jones (LJ) potential with a 13 Å cut-off was used to model short-

range interactions. The LJ parameters for the Na^+ counterions were taken from Joung et al[65]. LJ interactions between dissimilar atoms were calculated using geometric mixing rules, with the only exception being interactions between Na^+ counterions and water molecules. These interactions were modeled using the Lorentz-Berthelot mixing rules (similar to Joung et al[65]). A modified Particle-Particle Particle-Mesh (PPPM) solver[66] was used to calculate long-range electrostatic interactions with periodic boundary condition in the x and y directions, and fixed boundary condition in z direction.

Our initial configuration consisted of an array of counterions placed adjacent to fully extended PAA chains. Water molecules were added throughout the simulation domain. The SHAKE algorithm[67] was used to fix the bonds and angles of the SPC/E water molecules. Firstly, the system was run in a NP_zT (the subscript z indicates that only the simulation box height is allowed to change) ensemble using the Nosé-Hoover thermostat and barostat[68-69] in order to obtain the correct height of the simulation domain. The system temperature and pressure were maintained at 300K and 1 atmosphere respectively. The relaxation time for temperature and pressure were set to 0.1 ps and 1 ps respectively. This was followed by equilibration in the NVT ensemble using the Langevin thermostat[70]. The temperatures of the PE chains and the mobile species (water molecules and counterions) were separately maintained at 300K with a relaxation time of 0.1 ps for the thermostat. The atomic trajectories are calculated using the velocity-Verlet integrator with a time step of 2 fs. We monitored the autocorrelation function for average end-point height of the brushes $\langle z_e \rangle$ to check for equilibration. The equilibration times as well as the autocorrelation time scale for all simulations are provided in section S3 of the Supporting Information. A production run of 2 ns was performed for each case and the coordinates of each

atom were dumped at intervals of 200 fs and 1000 fs in separate files. The open source software OVITO[71] was used for visualization of the atomic trajectories.

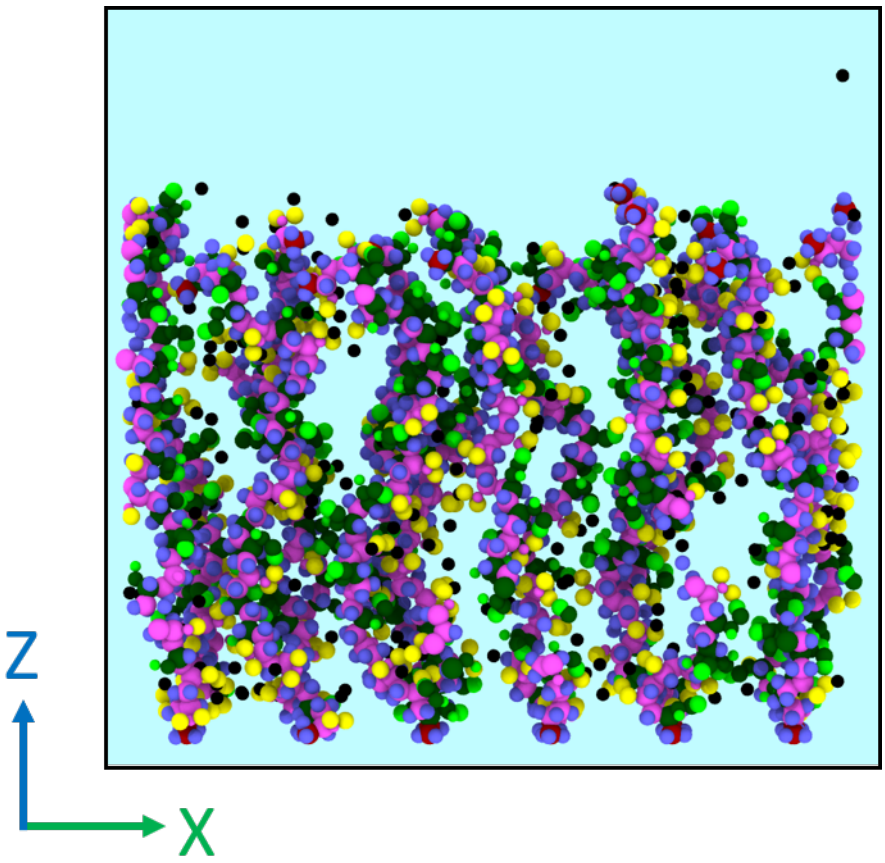

Figure 1: Snapshot depicting the partially ionized PAA brushes (f=1/2) for σ_g=0.1/σ^2. The black spheres represent the Na^+ counterions while other colors represent the different atom types of the PAA chains. Water molecules are not shown explicitly to improve visualization.

RESULTS AND DISCUSSION

PE Molecules: Brush Height and Chain Mobility

Figure 2 plots the end-to-end brush height (<z_e>) for various degrees of ionization (*f*) and grafting densities (σ_g) of the PAA brushes. For a given value of σ_g, we observe only a slight increase in the brush height with the degree of ionization (*f*) due to enhanced electrostatic repulsion between the chain segments as the effective charge of the brush segments increases with an increase in *f*. The brush height begins to saturate at higher values of *f*. Using coarse-grained MD simulations, Hao et al[56] also reported a weak increase in the brush height with respect to the degree of ionization for planar ring PE brushes at high grafting densities in presence of monovalent counterions. An increase in the grafting density implies that the brushes are forced to stretch out more in a direction perpendicular to the grafting surface, enforcing a larger value of the end-to-end brush height for a larger σ_g for a given *f*.

Fig. 2 also points that the brushes always remain in the swollen state for all values of *f*, since <z_e> >> ℓ (where $\ell = \sigma_g^{-1/2}$ is the lateral separation between adjacent chains). This behavior is consistent with the experiments of Swift et al[72], who reported no coil-to-globule transition for the PAA chains (in aqueous solution) below a molar mass of 16.5 kDa (corresponding to a degree of polymerization ≈230). They postulated that this behavior was a consequence of the inefficacy of the small chains to participate in intra-chain hydrogen bonding due to a lack of monomer-monomer contacts.

In a previous publication[60], we demonstrated that our all-atom MD-simulation predicted variation of the endpoint brush height (for the fully ionized brushes) with grafting density could be excellently recovered from the scaling laws of the non-linear osmotic brush regime[73-75]. However, in the present paper, the variation of the end-to-end brush height with respect to the

degree of ionization does not follow the scaling results of the non-linear osmotic brush regime. The scaling law massively overpredicts the change in brush height with respect to the degree of ionization (see section S4 in the Supporting Information). In fact, the mismatch between the scaling theory and the MD simulation results increases for lower degrees of ionization. This could be due to the lack of the consideration of excluded volume interactions between the PE segments in the scaling law of the non-linear osmotic brush regime, which becomes increasingly important at lower degrees of ionization. In fact, at high grafting densities (like the ones studied in the current paper), the excluded volume interactions dominate, and the brush height becomes almost independent of f (like an uncharged polymer brush).

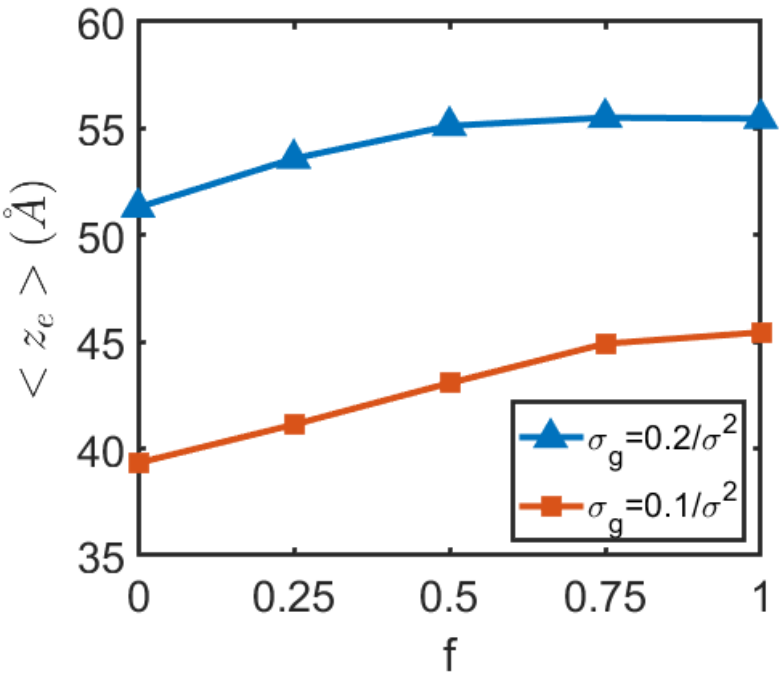

Figure 2: Variation in the end-point brush height with degree of ionization for different grafting densities.

Figure 3 quantifies the mobility of the PE brushes as a function of the degree of ionization. Accordingly, in Fig. 3(a) we plot the mean squared displacement (MSD) of the backbone Carbon atoms (numbered sequentially from 1 to 49 with 1 being the grafted Carbon atom and 49 being the non-grafted terminal Carbon atom) at t=100ps for different degrees of ionization and σ_g=0.1/σ^2. We can clearly observe the stratification in the mobility of the backbone Carbon atoms, with an increase in the mobility along the length of the chain (away from the grafting site). This behavior is expected, as the effect of the topological constraint due to grafting diminishes as one moves away from the grafting site. We see a sharp increase in the MSD of the last few Carbon atoms (near the non-grafted chain end) for all values of degree of ionization. This is due to a reduction in the steric effects from neighboring chains near the non-grafted chain ends. The thermal fluctuations near the chain ends cause different chains to attain different vertical heights and hence reduce the steric effects near the chain ends. The MSD of backbone carbon atoms decreases with an increase in the degree of ionization. This can be attributed to an enhancement in the average number of counterions condensed per PE chain. The condensed counterions form a sheath around the PE chains, like a jacket around a cylinder. The columbic repulsion between the condensed counterions of neighboring chains restricts the motion of the PE segments and thereby reduces the MSD of backbone atoms. Similar trend is observed at t=50ps (see section S5 in the Supporting Information). On the other hand, an increase in the grafting density forces the PE brushes to be even closer to one another enforcing a reduced mobility (or a smaller MSD) of a particular Carbon atom for a given *f* [compare the findings of Figs. 3 and S7].

Figure 3 (b) depicts the MSD of the non-grafted terminal Carbon atoms of the PE chains for different degrees of ionization and σ_g=0.1/σ^2. The slope of the MSD-vs-time curve decreases

due to the topological restrictions resulting from chain connectivity. Here too, we observe a reduction in the MSD with an increase in the degree of ionization and an increase in the grafting density (for reasons as explained before). Similar observations were made for the middle Carbon atom (the 25^{th} Carbon atom) of each chain (see section S5 in the Supporting Information).

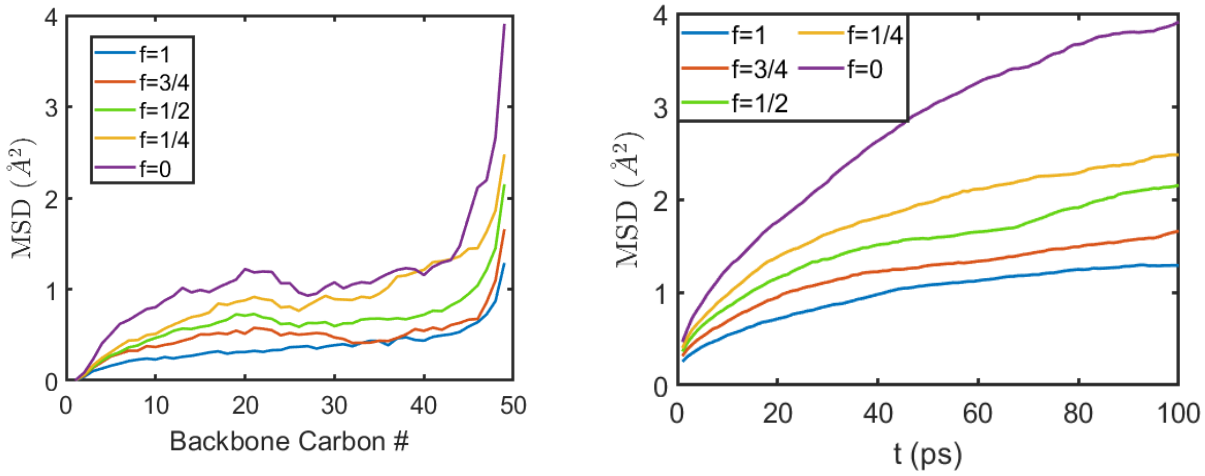

(a) (b)

Figure 3: (a) Stratification of the mean squared displacement (MSD) of backbone carbon atoms of the PE chains for various degrees of ionization at t=100ps for σ_g=0.1/σ^2, (b) MSD of the non-grafted terminal Carbon atom of the PE chains for various degrees of ionization for σ_g=0.1/σ^2. The result for the larger grafting density (σ_g=0.2/σ^2) is provided in Fig. S7 in section S7 in the Supplementary Material.

Counterions: Local Arrangement and Distribution

Quantification of the Extent of Counterion Condensation

In addition to the description of the change in the concentration as well as the transverse distribution of the PE-brush-supported counterions as functions of the grafting density and degree of ionization [see Figs. S5(a,b) and S6(a,b) and section S6 in the Supplementary Information], we intend to provide a more thorough understanding of the behavior, properties, and distributions of the counterions within the brushes as functions of *f*. Accordingly, in Figure 4(a), we depict the probability density [p(r)] of finding the nearest $O_{Carbocylate}$ atom at a distance *r* from a given counterion within the brushes for various degrees of ionization and σ_g=0.1/σ^2. This result will help to quantify the extent of counterion condensation on oxygen atoms of the COO^- groups ($O_{Carbocylate}$ atoms) of the PAA brushes. For all combinations of *f*, we observe a peak in the probability density at r~0.64σ (2.24 Å). This value is very close to the LJ diameter of Na^+ counterion (2.1595 Å), indicating counterion condensation. The peak value of probability density increases with degree of ionization, leading to a reduction in the probability density for higher values of *r*. This indicates a reduction in the average distance between the counterions and the nearest $O_{Carbocylate}$ atom (manifesting, as expected, in higher counterion condensation) with an increase in *f* or an increase in the charge of the PE brushes. A similar trend is observed for σ_g=0.2/σ^2 [see Figure S8(a)].

Next, in Figure 4 (b), we plot the cumulative distribution function (cdf) by integrating the probability density over a sphere of radius r [$\mathrm{cdf}(r) = \int_0^r 4\pi r^2 p(r) dr$]. This gives us the overall probability of finding the nearest $O_{Carboxylate}$ atom within a distance r from a given counterion. We observe that the cdf plateaus at a distance of r~0.75σ for all degrees of ionization and grafting density (depicted by black dashed line in the cdf plots). The value of the cdf at r=3.2 Å

or 0.914 σ (radius of the first solvation shell of Na^+) corresponds to the fraction of counterions condensed on the $O_{Carboxylate}$ atoms. We see a larger cdf plateau value corresponding to a larger f (or larger ionization), which is a consequence of the larger peak values in the probability density distribution [see Figure 4(a)]. A similar trend is observed for σ_g=0.2/σ^2 [see Figure S8(b)].

Figure 4(c) depicts the percentage of condensed counterions within the PE brush layer for various degrees of ionization and grafting densities. Most of the counterions (>90%) are condensed for the explored parametric range. We observe that the percentage of condensed counterions decreases for lower degrees of ionization. This is because the entropic cost of binding counterions to $O_{Carboxylate}$ atoms increases with a reduction in the degree of ionization. As a result, some of the counterions are able to break free of the enthalpically favorable electrostatic binding with the $O_{Carboxylate}$ atoms in order to reduce the net free energy of the system. In a recent coarse-grained MD study, Hao et al[56] also reported a decrease in the fraction of free (uncondensed) counterions with increasing degree of ionization for linear as well as ring PE brushes. We observe that the percentage of condensed counterions is typically larger at a higher grafting density, with the only exception at f=0.5.

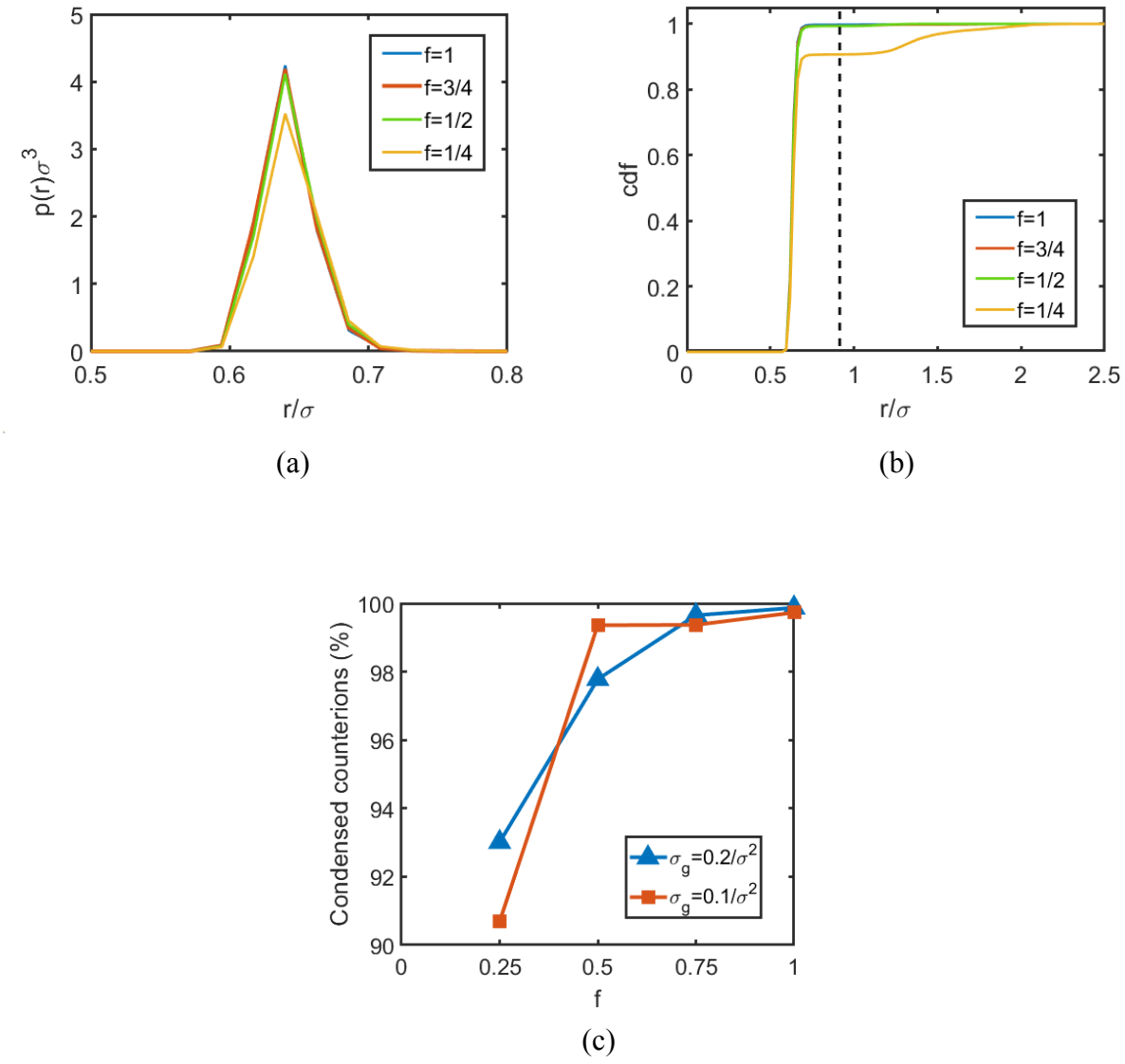

Figure 4: (a) Normalized probability distribution of finding the nearest $O_{Carboxylate}$ atom around Na^+ counterions within the PE brush layer for σ_g=0.1/σ^2 and (b) the cumulative distribution function (cdf) for scenario depicted in (a). In (a) and (b), results are shown for different degrees of ionization. (c) The percentage of counterions (present within the PE brush layer) condensed on $O_{Carboxylate}$ atoms for different degrees of ionization and grafting densities.

Quantification of "Water-in-Salt" Like Behavior

In our previous paper considering the all-atom MD simulations of fully ionized PAA brushes, we had established a unique *water-in-salt-like* scenario within the PE brushes, where the solvation water of the brush-supported counterions got replaced by the COO^- functional group of the PE[60]. This *water-in-salt-like* scenario was quantified by studying the solvation structure of the counterions (that gave a sense to what extent the solvation water was replaced by the PE functional group) and the condition where the counterion-PE-functional-group complex (acting as the effective "salt") overwhelmed water in terms of volume and weight[60].

Here we quantify the similar *water-in-salt-like* scenarios as a function of the degree of ionization of the PE brushes and the grafting density. Accordingly, in Figures 5(a) and (c), we depict the solvation structure of the counterions within the PE brushes for different degrees of ionization and grafting densities. Inside the brushes, the solvation water of the counterions (Oxygen of water molecules or O_{Water} atoms to be specific) can be partially replaced by $O_{Carboxylate}$ atoms (Oxygen of COO^- group), $O_{Carbonyl}$ atoms (double bonded Oxygen of COOH group) as well as $O_{Hydroxyl}$ atoms (single bonded Oxygen of COOH group). Such a replacement of the solvation water by the $O_{Carbonyl}$ or $O_{Hydroxyl}$ atoms, which is not relevant for the case of fully ionized PE brushes[60], is only relevant when the PE brushes are only partially ionized and contains non-dissociated COOH group. The contribution of $O_{Carbonyl}$ and $O_{Hydroxyl}$ atoms in replacing the water from the solvation shell of counterion is much smaller than that of $O_{Carboxylate}$ atoms, for all degrees of ionization. This happens because the carboxylate group (COO^-) has a net negative charge whereas the oxygens on the carboxylic acid group (COOH) only carry partial charges (carboxylic acid group is neutral as a whole), thereby ensuring a much larger attraction between the carboxylate group and the counterions as compared to that between the oxygen of the COOH and counterions. This enhanced attraction allows the COO^- group to show a much

larger tendency to bind strongly with the counterion and in the process lead to a much more effective replacement of the solvation water of the counterion. Of course, the replacement of water molecules always occurs in a way that preserves the total solvation number of the Na^+ counterions (~6). The contribution of $O_{Carboxylate}$ atoms increases with *f*, whereas that of $O_{Carbonyl}$ and $O_{Hydroxyl}$ atoms decreases with *f*. This is simply due to the increase in the ratio of ionized groups (COO^-) to protonated groups (COOH) at higher degrees of ionization. The total number of water molecules within the first solvation shell ($r \leq 3.2$ Å) of Na^+ ions shows different trends with respect to the degree of ionization, depending on the grafting density. At lower grafting density ($\sigma_g = 0.1/\sigma^2$), the number of solvation water molecules first decreases with *f* ($0.25 \leq f \leq 0.5$) and then becomes almost invariant with *f* ($0.5 \leq f \leq 1$). However, this invariance is not witnessed at high grafting density ($\sigma_g = 0.2/\sigma^2$), where the number of solvation water molecules monotonically decreases with the degree of ionization. An increase in the $O_{Carboxylate} - Na^+$ coordination number with degree of ionization for PAA chains in solution was also reported in Ref. 51. This is consistent with the increase in number of $O_{Carboxylate}$ atoms within the first hydration shell of Na^+ ions with *f*, shown in Figures 5 (a) and 5(c). The average solvation number of Na^+ ions within the brushes is a resultant of the contributions from the condensed as well as the uncondensed Na^+ counterions. The solvation structure of the condensed and uncondensed counterions for $\sigma_g = 0.1/\sigma^2$ is compared and discussed in Fig. S15 and section S8 in the Supplementary Material.

Figures 5 (b) and (d) depict the mass and volume ratios of the "salt" to water molecules within the PE brushes for various degrees of ionization and grafting density. Very similar to our previous paper[60], in our system, the "salt" is formed by the counterions and the charged PE segments. Therefore, the Na^+ counterions act as the cations and the ionized monomers [$-CH_2-$

CH(COO^-)-] act as the anions. As expected, the "salt" to water ratios (by mass and volume) increase monotonically with the degree of ionization since larger *f* implies the presence of a larger number of ionized segments (-COO^-) that can form the "salt" with the counterions. For the higher grafting density ($\sigma_g = 0.2/\sigma^2$), we observe that both the mass and volume ratios cross 1 at approximately *f*=0.5. Thus, beyond *f*=0.5, the "salt" supersedes water by both mass and volume, giving rise to water in salt like scenarios. However, such a scenario is not witnessed for the lower grafting density ($\sigma_g = 0.1/\sigma^2$), where the mass ratio remains less than 1, even at full ionization of the brushes (*f*=1). This is because of the smaller counterion concentrations (and hence "salt" concentration) witnessed at lower grafting density (see Fig. S5).

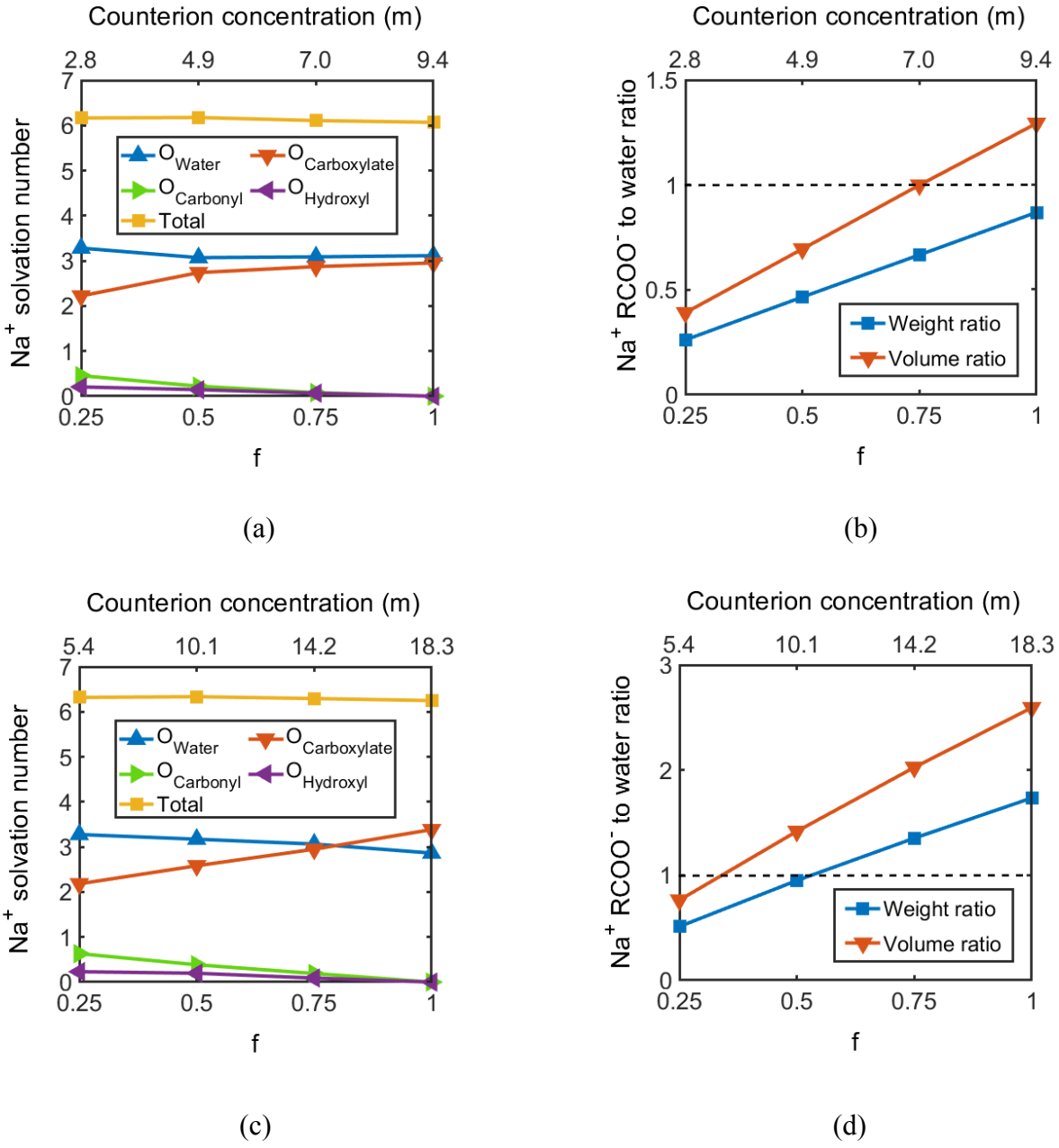

Figure 5: Variation in the solvation structure of Na^+ counterions (within the PE brush layer) with degree of ionization for (a) $\sigma_g=0.1/\sigma^2$ and (c) $\sigma_g=0.2/\sigma^2$. 'Salt'-to-water mass and volume ratios for various degrees of ionization for (b) $\sigma_g=0.1/\sigma^2$ and (d) $\sigma_g=0.2/\sigma^2$. Here "salt" refers to Na^+ $RCOO^-$ (R: $-CH_2-CH-$).

Brush-induced Variation of the Counterion-water-oxygen Radial Distribution Function (RDF)

Figures 6 (a) and (b) plot the Na^+ - O_w RDF (O_w represents Oxygen of water molecules) of counterions within the brushes for various degrees of ionization and grafting densities. We also provide the Na^+ - O_w RDF in bulk for comparison. The height of the peak corresponding to the first solvation shell of the counterions reduces inside the brushes (compared to bulk). This is due to the partial replacement of water molecules within the first solvation shell of the counterions by $O_{Carboxylate}$, $O_{Carbonyl}$ and $O_{Hydroxyl}$ atoms.

At a higher grafting density ($\sigma_g = 0.2/\sigma^2$) [see Fig. 6(b)], the height of this peak, corresponding to the first solvation shell, reduces monotonically with an increasing degree of ionization. This can be explained as follows: Firstly, there is a reduction in the number of water molecules within the first solvation shell of the Na^+ counterions with an increase in *f* [see Fig. 5(c) and the related discussions]. Secondly, the overall density of water within the brushes itself increases with the degree of ionization (see section on mass density of water and Figure 9). This reduces the height of the peak even further as the RDF is normalized with respect to the overall density of water within the brushes.

At a lower grafting density ($\sigma_g = 0.1/\sigma^2$), the height of this peak, corresponding to the first solvation shell, initially decreases with an increase in the degree of ionization ($0.25 \leq f \leq 0.5$). Again, this is due to the depletion of water molecules within the first solvation shell of Na^+ in this range of *f* ($0.25 \leq f \leq 0.5$) [see Fig. 5(a)] coupled with an increase in the overall density of water molecules (within the brushes) with *f*. However, beyond $f=0.5$, the number of water molecules within the first solvation shell of the counterions becomes almost invariant of the degree of ionization (increases very slightly with increase in *f*) [see Fig. 5(a)]. Of course, the water density within the brushes still increases with *f*. The resultant of these two effects is that

the peak heights corresponding to the first solvation shell of Na^+ become very close and vary non-monotonically with respect to f for $0.5 \leq f \leq 1$.

The Na^+ - O_w RDFs plotted in Figure 6 have contributions from both condensed and uncondensed counterions. In Fig S16 and section S9 in the Supplementary Material, we discuss the variation of the Na^+ - O_w RDF for uncondensed Na^+ ions (for $\sigma_g = 0.1/\sigma^2$) to shed light on the differences between the hydration of condensed and free (uncondensed) counterions within the brushes.

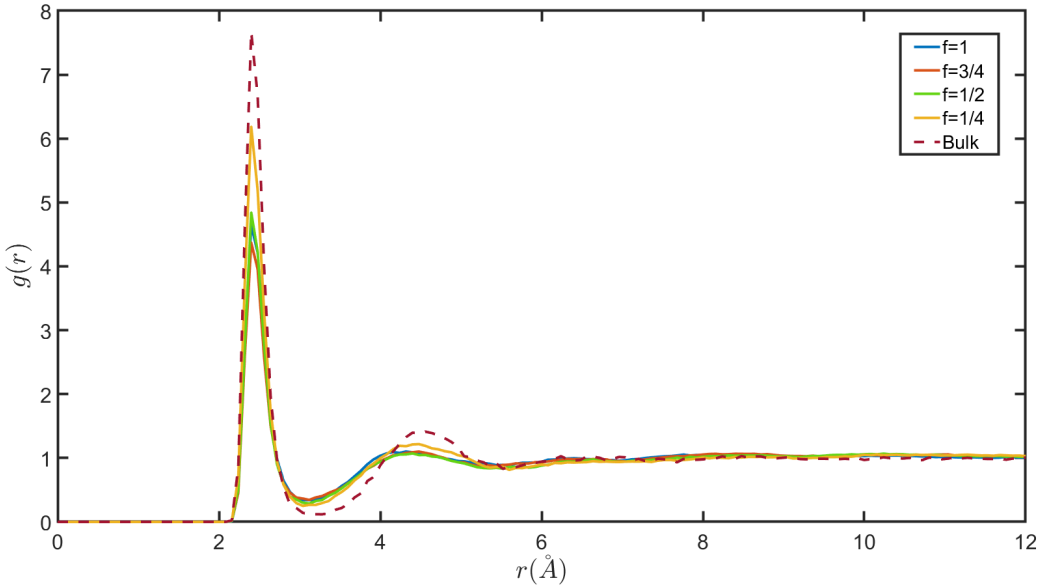

(a)

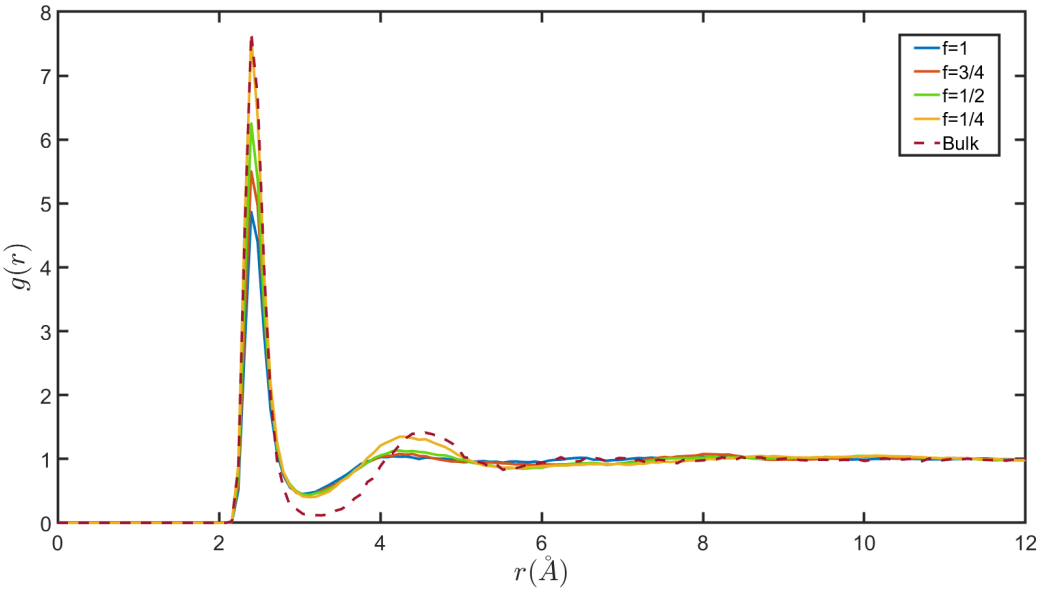

(b)

Figure 6: Na^+ - O_w (O_w represents Oxygen of water molecules) RDF within the PE brush layer for various degrees of ionization for (a) σ_g=0.1/σ^2 and (b) σ_g=0.2/σ^2. Bulk Na^+ - O_w RDF is also provided for comparison (dashed line).

Mobility of the counterions within the PE brushes

Our previous all-atom MD simulation paper had identified a significant reduction in the mobility (quantified through the corresponding mean squared displacements or MSDs) of the counterions within the densely grafted PE brushes owing to the large confinement effect introduced by the densely grafted brushes as well as the strong electrostatic attraction between the completely ionized PE brushes and the counterions[60]. Here we study the effect of the varying degree of ionization on the counterion mobility. For that purpose, in Figure 7 we depict the MSD of the Na^+ counterions within the brushes for different degrees of ionization and σ_g=0.1/σ^2. The slope of the MSD-vs-time curves decreases with time and the MSD eventually saturates to a constant value. This indicates that the counterions are unable to diffuse freely. This happens due to a combination of electrostatic binding with the PE segments and brush-induced nanoconfinement. For a given grafting density, the counterion mobility increases with decrease in the degree of ionization due to a decrease in the percentage of bound counterions (see section on counterion condensation and Figure 4). Bound counterions are condensed on the $O_{Carboxylate}$ atoms and lose much of their mobility due to strong columbic interactions. The counterion mobility is much smaller at a higher grafting density ($\sigma_g = 0.2/\sigma^2$) due to enhancement in the percentage of bound counterions (typically) and a stronger brush induced confinement [compare the findings of Figs. 7 and S9 in the Supplementary Material].

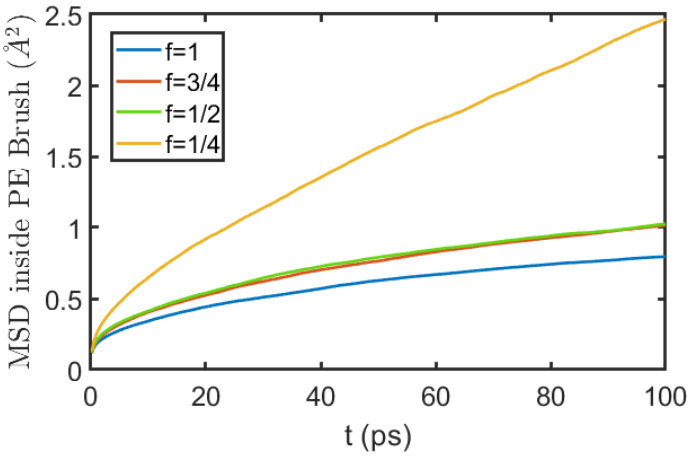

Figure 7: Mean squared displacement (MSD) of Na^+ counterions within the PE brush layer for various degrees of ionization for σ_g=0.1/σ^2. The result for the larger grafting density (σ_g=0.2/σ^2) is provided in Fig. S9 in section S7 in the Supplementary Material.

Water: Local Arrangement and Distribution

Brush-induced Variation of the water-oxygen-water-oxygen Radial Distribution Function (RDF)

Figure 8 depicts the $O_w - O_w$ (water-oxygen-water-oxygen) RDF of water molecules inside the brushes for various degrees of ionization and $\sigma_g=0.1/\sigma^2$. $O_w - O_w$ RDF of bulk water is also provided for comparison. The peak height corresponding to the first solvation shell increases drastically within the uncharged brushes (f=0) as compared to bulk. This is because the overall density of water molecules within the uncharged brushes is significantly smaller as compared to bulk (see section on mass density of water and Figure 9) and the RDF is normalized with respect to the overall water density.

The RDF shifts towards the right within the brushes as compared to bulk. This is because the PE chains and counterions occupy spaces between the water molecules causing them to drift further away from each other. The rightward shift in RDF is more prominent at higher degrees of ionization due to the corresponding enhanced counterion concentration within the brushes.

The peak height corresponding to the first solvation shell decreases with an increase in the degree of ionization. This is because of the partial replacement of water molecules by counterions inside the first solvation shell of water. Increase in degree of ionization increases the counterion concentration within the brushes, resulting in a more enhanced replacement of water molecules within the first solvation shell of water. Moreover, the overall water density within the brushes increases with the degree of ionization, also resulting in lowering of the first peak height with f (the RDF is normalized with respect to the overall density of water molecules).

The $O_w - O_w$ RDF within the brushes plotted in Figure 8 has contributions from both bound and free water molecules. A water molecule present inside the first solvation shell of a Na^+ ion ($r \leq 3.2$ Å) is considered to be bound. Otherwise it is considered as a free water

molecule. The $O_w - O_w$ RDFs for both bound and free water molecules are plotted separately for comparison in Figure S17. This will help to explain the differences between the local structure of the bound and free water molecules within the brushes.

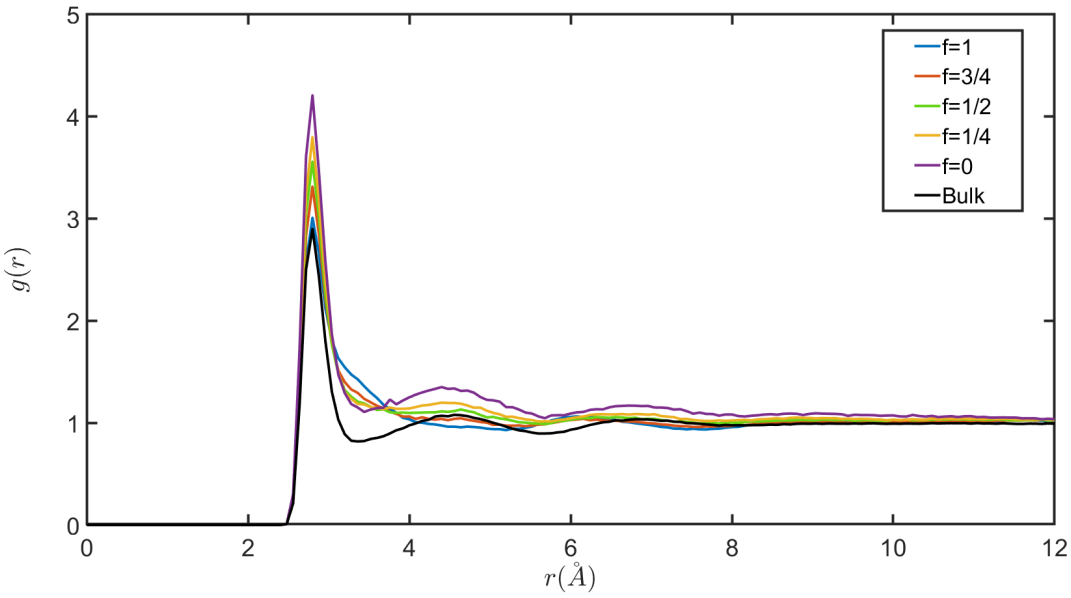

Figure 8: O_w-O_w RDF of water molecules within the PE brush layer for various degrees of ionization for σ_g=0.1/σ^2. Bulk O_w-O_w RDF is also provided for comparison. The result for the larger grafting density (σ_g=0.2/σ^2) is provided in Fig. S10 in section S7 in the Supplementary Material.

Water density within the PE Brushes

In Figure 9, we plot the local mass density of water molecules as a function of the z coordinate (z=0 is the grafting plane) for various degrees of ionization (*f*) and σ_g=0.1/σ^2. The result for the higher grafting density (σ_g=0.2/σ^2) is shown in Fig. S11 in the Supplementary Material. The water mass density drastically decreases within the brushes as compared to that in the bulk, as has been reported in our previous paper[60]. Interestingly, inside the brushes, the mass density of water increases with f for both the grafting densities. Two factors are at play here. On one hand, increasing the degree of ionization leads to a significant increase in the number of counterions trapped within the brushes, as evident by the much larger values of counterion concentration for such degrees of ionization (see Figure S5). For example, the counterion concentration for $\sigma_g = 0.2/\sigma^2$ at *f*=1 is 18.33 m i.e., there is 1 counterion for approximately every 3 water molecules. Such a massive increase in counterion concentration leads to steric effects ensuring that there is lesser space available for the water molecules. On the other hand, an increase in the degree of ionization increases the number of water molecules required to solvate the counterions. Thus, more water molecules get trapped inside the brushes to cater to the solvation requirements of the counterions.

These two effects counter each other. While steric effects tend to reduce the number of water molecules by reducing the space available for the water molecules, the enhanced counterion solvation requirements warrant an increase in the number of water molecules present inside the brushes. We observe that the counterion solvation requirements dominate the steric effects for both values of grafting densities and dictate an enhancement in the mass density of water inside the brushes with an increase in the degree of ionization. This establishes a highly fascinating scenario: a progressive increase in the degree of ionization effectively pulls in more

amounts of species in a given available volume as manifested by the simultaneous increase in the counterion concentration and water mass density. In other words, this suggests that a charged PE brush is capable of "packing" more amounts of species (counterions and water) within the layer that it forms as compared to the layer formed by an uncharged (or weakly charged) polymer brush.

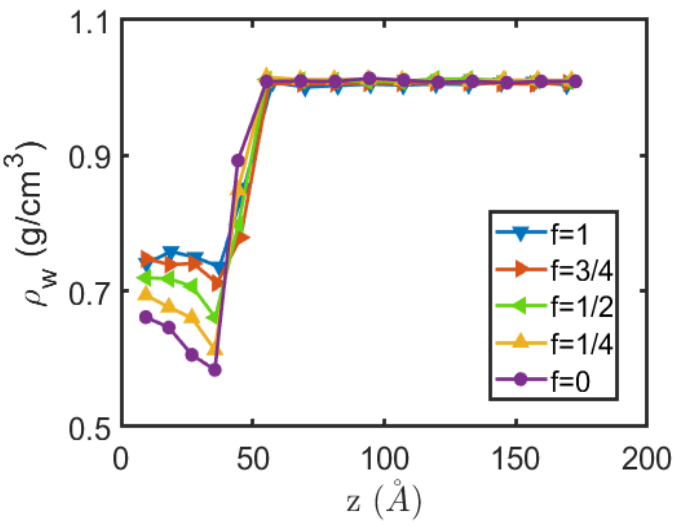

Figure 9: Transverse variation of mass density of water molecules for various degrees of ionization for σ_g=0.1/σ^2.

Brush-induced Variation of Static Dielectric Constant of Water

Figure 10 plots the static dielectric constant of water molecules (normalized by its bulk value), $\bar{\epsilon_r} = \frac{\epsilon_r(0)}{[\epsilon_r(0)]_{Bulk}}$ within the brushes for various values of degree of ionization (f) and grafting densities. Here $\epsilon_r(0)$ is the dielectric constant of water molecules within the brushes at zero frequency and $[\epsilon_r(0)]_{Bulk}$ is the dielectric constant of bulk water at zero frequency. Our previous study had reported a significant decrease in $\bar{\epsilon_r}$ within the brushes for the fully ionized brushes[60]. Here we study the role of *f* and σ_g in this reduction of $\bar{\epsilon_r}$. The static dielectric constant of water molecules was calculated using the linear response theory[76] as:

$$\epsilon_r(0) = 1 + \frac{1}{3k_BT\epsilon_0 V}(< \mathbf{M}^2 > - < \mathbf{M} >^2), \quad (1)$$

where k_BT is the thermal energy, ϵ_0 is the permittivity of free space, V is the volume under consideration and **M** is the total dipole moment of water molecules in volume V.

A non-monotonic variation in the dielectric constant of water with *f* is observed for both values of grafting density. There are two factors at play here. Firstly, the mass density (and hence the number density) of water molecules within the brushes increases with the degree of ionization (see section on mass density of water and Figure 9). This increases the dielectric polarization density in the presence of an electric field as there is greater number of water molecules (per unit volume) available to be polarized in the first place. Secondly, the percentage of bound water molecules also increases with the degree of ionization. A water molecule is considered to be bound if it is present within the first solvation shell ($r \leq 3.2$ Å) of a Na^+ counterion. This trend is depicted on the right axis in Figures 10 (a) and (b). An increase in the percentage of bound water molecules decreases the dielectric constant of water due to the inability of bound water molecules to polarize freely in the presence of an electric field.

Clearly, the two effects oppose each other. The resultant of the two effects leads to the observed non-monotonic variation in the dielectric constant of water (within the brushes) with the degree of ionization. At lower grafting density ($\sigma_g = 0.1/\sigma^2$), the mass density effect dominates at lower values of f ($0 \leq f \leq 0.75$), while the effect associated with the enhancement in fraction of bound water molecules dominates at higher values of f ($0.75 \leq f \leq 1$). This leads to an initial enhancement in the dielectric constant of water followed by a reduction with increase in the degree of ionization. However, we observe a completely opposite trend at higher grafting density. For $\sigma_g = 0.2/\sigma^2$, we witness a decrease in the dielectric constant of water at low to moderate degrees of ionization followed by a slight increase at high degrees of ionization.

This finding points to a most interesting scenario where a fundamental property of water such as the *static dielectric constant* could be regulated in a most unique fashion within a layer of PE brushes by tuning the degree of ionization and the grafting density of the brushes.

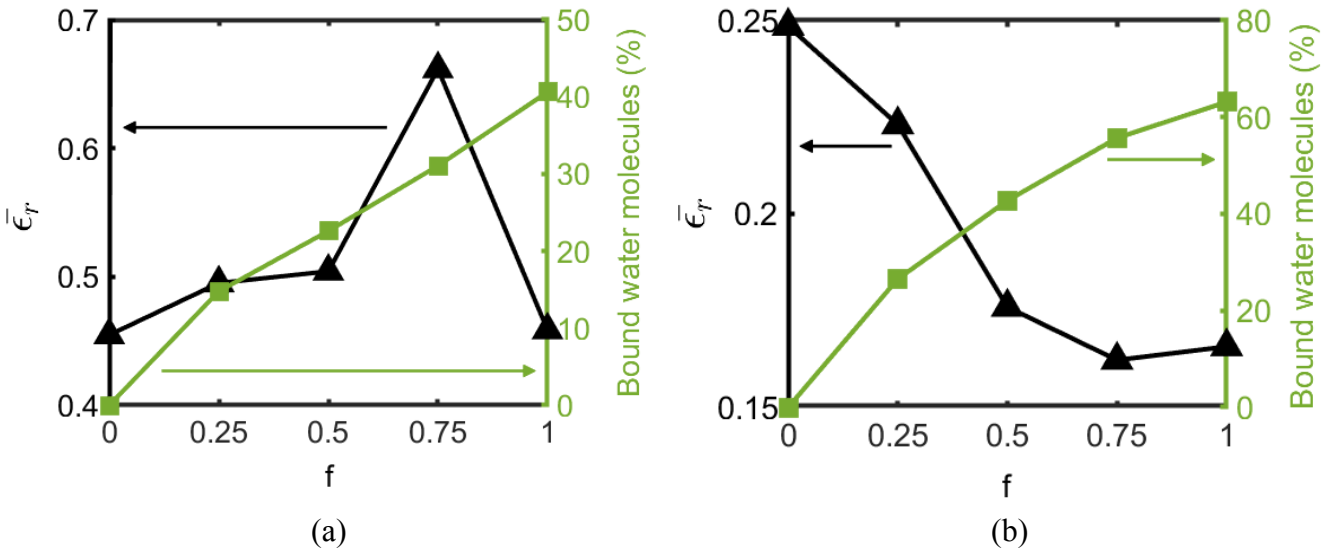

(a) (b)

Figure 10: Left axis- Static dielectric constant of water molecules (normalized with respect to bulk value) within the brushes for various degrees of ionization. Right axis- Variation in the percentage of bound water molecules within the PE brush layer for various degrees of ionization. Results are shown for (a) σ_g=0.1/σ^2 and (b) σ_g=0.2/σ^2.

Variation of the Hydrogen-Bond Network within the PE Brushes

Figure 11 plots the transverse variation in average number of hydrogen bonds formed by water molecules (per water molecule) (n_{HB}) for various degrees of ionization and $\sigma_g=0.1/\sigma^2$. The transverse variation in average number of hydrogen bonds formed by water molecules with other water molecules (per water molecule) ($n_{HB,w}$) is also plotted. The result corresponding to a larger grafting density ($\sigma_g=0.2/\sigma^2$) is provided in Fig. S12. Water molecules can form hydrogen bonds with other water molecules as well as the polyelectrolyte chains. Various atoms on the pendant groups of the PAA chains can form hydrogen bonds with water molecules. These include the $O_{Carboxylate}$, $O_{Carbonyl}$, $O_{Hydroxyl}$ and $H_{Hydroxyl}$ (Hydrogen of COOH group) atoms. Thus, PAA functional groups can behave like hydrogen bond acceptors (via $O_{Carboxylate}$, $O_{Carbonyl}$ and $O_{Hydroxyl}$ atoms) as well as hydrogen bond donors (via $H_{Hydroxyl}$ atoms). A hydrogen bond (between water-water or water-PE functional group) is considered to exist if the distance between the donor and acceptor Oxygen atoms is less than 3.4 Å, the distance between the participating Hydrogen atom and acceptor Oxygen atom is less than 2.425 Å, and the angle between participating Hydrogen atom−donor Oxygen atom−acceptor Oxygen atom is less than 30°[77-78].

There is a significant reduction in hydrogen bonding between water molecules within the brushes (as compared to bulk) even for the case of uncharged brushes (f=0). This is because water molecules form hydrogen bonds with the PAA chains at the expense of water-water hydrogen bonds. We observe that increasing the degree of ionization increases the average number of hydrogen bonds between water molecules and PAA functional groups per PAA chain ($n_{HB,PAA-Water}$) [see Fig. 11(c)]. Such an increase in water – PAA hydrogen bonding improves the hydrophilicity of the brushes and is commensurate with the enhanced brush height at higher degrees of ionization (see Fig. 2). In their all-atom MD study, Sappidi et al[51] also observed an

increase in the number of water – PAA hydrogen bonds with the degree of ionization of atactic PAA chains in solution. We witness a decrease in $n_{HB,w}$ with an increasing degree of ionization. This can be attributed to the increase in counterion concentration within the brushes. The Na^+ counterions act as structure breakers and undermine the hydrogen bond network between the water molecules.

The aforementioned effects compete with each other. On one hand, an increase in the degree of ionization increases the hydrogen bonding between water and PAA chains ($n_{HB,\ PAA\text{-}Water}$). On the other hand, it leads to a reduction in the hydrogen bonding between water molecules ($n_{HB,w}$). However, the change in number of hydrogen bonds between water molecules and PAA chains (with the degree of ionization) is much smaller as compared to the change in number of hydrogen bonds formed by water molecules with each other. Therefore, the resultant of the two effects is an overall decrease in the number of hydrogen bonds per water molecule (n_{HB}) with increasing degree of ionization (for both values of σ_g).

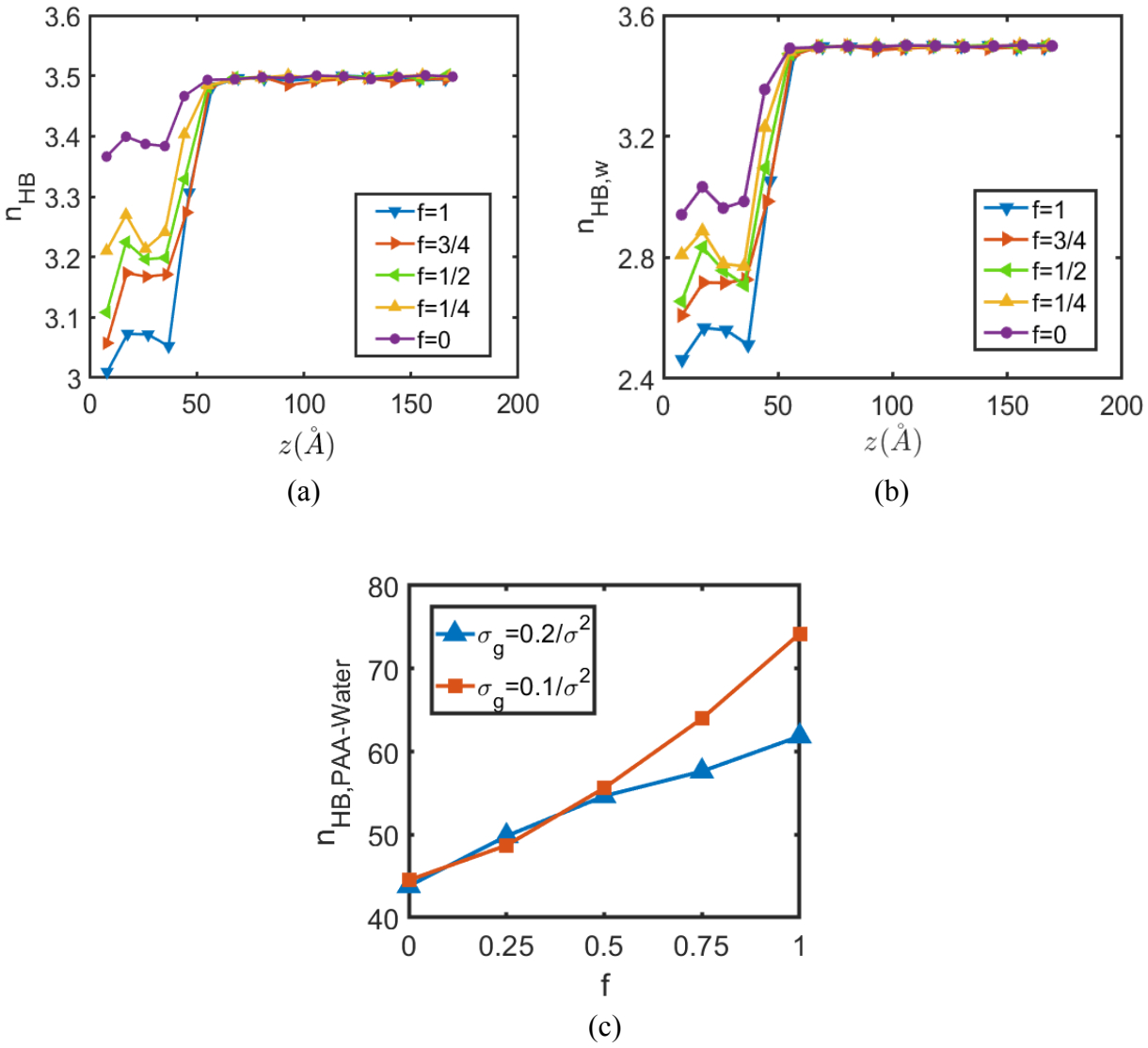

Figure 11: (a) Transverse variation in number of hydrogen bonds per water molecule n_{HB} with degree of ionization for σ_g=0.1/σ^2, (b) Transverse variation in number of hydrogen bonds between water molecules (per water molecule) $n_{HB,w}$ with degree of ionization for σ_g=0.1/σ^2, (c) Average number of hydrogen bonds between PAA functional groups and water molecules (per PAA chain) $n_{HB,PAA-Water}$ for various degrees of ionization and grafting densities.

Orientational Tetrahedral Order Parameter of Water Molecules within the PE Brushes

Figure 12 plots the probability distribution of the orientational tetrahedral order parameter (q) of water molecules[62] within the brushes for various degrees of ionization and σ_g=0.1/σ^2. The result corresponding to a larger grafting density (σ_g=0.2/σ^2) is provided in Fig. S13. q=1 corresponds to a perfectly tetrahedral arrangement of water molecules. Smaller values of q represent larger deviations from the local tetrahedral arrangement. We observe that the presence of brushes causes a significant change in the probability distribution. This happens even if the brushes are uncharged (f=0). The presence of brushes causes a reduction in the hydrogen bonding (as compared to bulk) between water molecules ($n_{HB,w}$), thereby significantly distorting the local tetrahedral arrangement of water. This shifts the probability distribution towards lower values of q within the brushes. The shift towards lower values of q is more pronounced at higher grafting density, as the hydrogen bond network between water molecules is much more severely affected at higher values of σ_g (as seen by comparing of the findings of Figs. 12 and S13).

The mean value of q remains relatively unaffected with the degree of ionization. However, the height of the probability distribution peak increases with an increase in the degree of ionization. As a result, the distribution becomes narrower and its variance decreases. This suggests that there is a higher energy penalty to fluctuations away from the mean local arrangement of water molecules at higher degrees of ionization. Such penalties could result from the presence of strong electric fields generated by the enormous counterion concentration within the brushes.

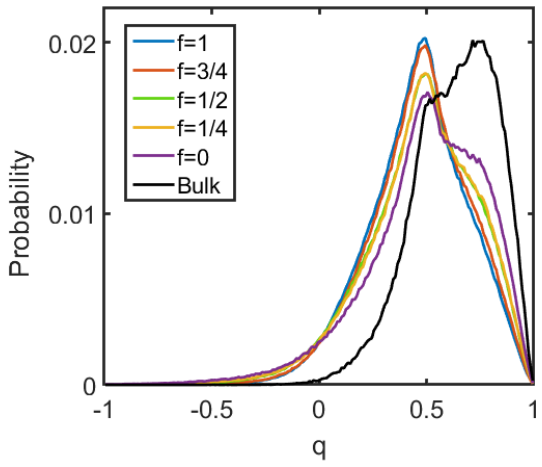

Figure 12: Probability distribution of orientational tetrahedral order parameter (q) of water molecules within the PE brushes for various degrees of ionization for σ_g=0.1/σ^2. Probability distribution of q for bulk SPC/E water is also provided for comparison.

Mobility of the water molecules within the PE brushes

Our previous paper had identified a significant reduction of the mobility of the water molecules (quantified by the corresponding MSDs) within the fully-ionized PE brushes owing to the large confinement effect induced by the densely grafted PE brushes as well as the significant dipolar interactions between water molecules and the charged PE brushes[60]. Here we quantify the water mobility within the PE brushes as functions of the degree of ionization and σ_g=0.1/σ^2. . For that purpose, in Figure 13 we depict MSDs of water molecules within the brushes as a function of time for various degrees of ionization and σ_g=0.1/σ^2. The long-time slope of the MSD-vs-time curves decreases with an increase in the degree of ionization and grafting density, indicating some form of confinement effect that is hindering the water molecules from diffusing freely. The reduction in water mobility with increasing degree of ionization can be explained via electrostatic interactions. With an increase in *f*, the percentage of water molecules bound to the counterions increases (see section on static dielectric constant of water and Figure 10). A majority of these counterions are in turn condensed on the $O_{Carboxylate}$ atoms of the PAA brushes. In fact, the percentage of condensed counterions itself increases with *f* (see section on counterion condensation and Figure 4). As a result, the water molecules become much less mobile with increased ionization of the PE chains.

We witness a significant reduction in MSD of water molecules within the brushes (as compared to bulk) even for *f*=0. This indicates that electrostatic binding to the counterions is not the only reason for reduction in water mobility within the brushes. There is a tremendous nanoconfinement effect created by the presence of the brushes alone (even if they are uncharged). The reason for this is twofold. Firstly, the brushes create a form of lateral confinement due to their unique topology. Secondly, the water molecules form hydrogen bonds

with the pendant groups attached to the PE backbone. This further restricts their mobility as the PE chains are tethered to a substrate and cannot move freely (see Figure 3). Similar trends are observed for the case of higher grafting density, i.e., $\sigma_g=0.2/\sigma^2$ (see Fig. S14).

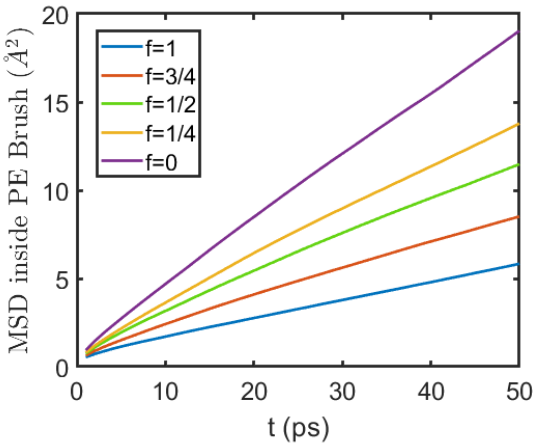

Figure 13: Mean squared displacement (MSD) of water molecules within the PE brushes for various degrees of ionization for σ_g=0.1/σ^2.

CONCLUSIONS

Changes in the properties of PE brushes along with the local arrangement and distribution of counterions and water molecules with the degree of ionization of the brushes are quantified via an all-atom MD framework elucidating the effects of the variation of degree of ionization and the grafting density of the PE brushes. The brush height shows a weak increase with the degree of ionization due to enhanced electrostatic repulsion between the chain segments. The chain mobility, quantified via the MSD of the backbone Carbon atoms, decreases with an increase in the degree of ionization, due to an enhancement in the number of condensed counterions per PE chain. We witness an enhancement in the percentage of condensed condensation along with a reduction in the counterion mobility with an increase in the degree of ionization. This is accompanied by an increase in the mass density of water within the brushes and a reduction in the water mobility and hydrogen bonding between water molecules (per water molecule). Several other changes in the PE brush microstructure are quantified via shifts in the counterion-water and water-water RDFs as well as the probability distribution of the orientational tetrahedral order parameter of water. Moreover, the static dielectric constant of water molecules shows a non-monotonic trend with respect to the degree of ionization, depending on the grafting density of the brushes.

SUPPORTING INFORMATION

This article contains supporting information.

ACKNOWLEDGEMENTS

This work has been supported by the Department of Energy Office of Science grant DE-SC0017741. The authors would like to thank Dr. Peter W. Chung at the University of Maryland, College Park for providing computational resources to carry out some of the simulations. Few simulations and analyses were performed on the high-performance cluster Deepthought2.

DECLARATION OF INTERESTS

The authors declare no conflict of interest.

REFERENCES

1. Kwon, H. J.; Osada, Y.; Gong, J. P. Polyelectrolyte Gels-Fundamentals and Applications. *Polym. J.* **2006**, 38, 1211–1219.
2. Hong, W.; Zhao, X.; Suo, Z. Large Deformation and Electrochemistry of Polyelectrolyte Gels. *J. Mech. Phys. Solids* **2010**, 58, 558–577.
3. Harland, R. S.; Prud'homme, R. K. *Polyelectrolyte Gels: Properties, Preparation, and Applications*; Washington, DC (United States), American Chemical Society, 1992.
4. Dobrynin, A. V.; Rubinstein, M. Theory of Polyelectrolytes in Solutions and at Surfaces. *Prog. Poly. Sci.* **2005**, 30, 1049–1118.
5. Muthukumar, M. 50th Anniversary Perspective: A Perspective on Polyelectrolyte Solutions. *Macromolecules* **2017**, 50, 9528–9560.
6. Barrat, J. L.; Joanny, J. F. Theory of Polyelectrolyte Solutions. *Adv. Chem. Phys.* **1996**, 94, 1–66.
7. Sing, C. E.; Olvera de la Cruz, M.; Polyelectrolyte Blends and Nontrivial Behavior in Effective Flory–Huggins Parameters. *ACS Macro Lett.* **2014**, 3, 698–702.
8. Gao, L.; Seliskar, C. J. Formulation, Characterization, and Sensing Applications of Transparent poly (vinyl alcohol)− Polyelectrolyte Blends. *Chem. Mater.* **1998**, 10, 2481–2489.
9. Zeglio, E.; Vagin, M.; Musumeci, C.; Ajjan, F. N.; Gabrielsson, R.; Trinh, X. T., Son, N. T.; Maziz, A.; Solin, N.; Inganäs, O. Conjugated Polyelectrolyte Blends for Electrochromic and Electrochemical Transistor Devices. *Chem. Mater.* **2015**, 27, 6385–6393.

10. Chen, G.; Sachar, H. S.; Das, S. Efficient Electrochemomechanical Energy Conversion in Nanochannels Grafted with End-charged Polyelectrolyte Brushes at Medium and High Salt Concentration. *Soft Matter* **2018**, 14, 5246–5255.
11. Sachar, H. S.; Sivasankar, V. S.; Das, S. Electrokinetic Energy Conversion in Nanochannels Grafted with pH-responsive Polyelectrolyte Brushes Modelled using Augmented Strong Stretching Theory. *Soft Matter* **2019**, 15, 5973–5986.
12. Ali, M.; Yameen, B.; Neumann, R.; Ensinger, W.; Knoll, W.; Azzaroni, O. Biosensing and Supramolecular Bioconjugation in Single Conical Polymer Nanochannels. Facile Incorporation of Biorecognition Elements into Nanoconfined Geometries. *J. Am. Chem. Soc.* **2008**, 130, 16351–16357.
13. Umehara, S.; Karhanek, M.; Davis, R. W.; Pourmand, N. Label-Free Biosensing with Functionalized Nanopipette Probes. *Proc. Natl. Acad. Sci. U. S. A.* **2009**, 106, 4611–4616.
14. Motornov, M.; Sheparovych, R.; Lupitskyy, R.; MacWilliams, E.; Hoy, O.; Luzinov, I.; Minko, S. Stimuli□Responsive Colloidal Systems from Mixed Brush□Coated Nanoparticles. *Adv. Funct. Mater.* **2007**, 17, 2307–2314.
15. ShamsiJazeyi, H.; Miller, C. A.; Wong, M. S.; Tour, J. M.; Verduzco, R. Polymer□Coated Nanoparticles for Enhanced Oil Recovery. *J. Appl. Polym. Sci.* **2014**, 131, 40576.
16. Yang, Q.; Li, L.; Zhao, F.; Han, H.; Wang, W.; Tian, Y.; Wang, Y.; Ye, Z.; Guo, X. Hollow Silica–Polyelectrolyte Composite Nanoparticles for Controlled Drug Delivery. *J. Mater. Sci.* **2019**, 54, 2552–2565.
17. Saraswathy, M.; Gong, S. Recent Developments in the Co-Delivery of Sirna and Small Molecule Anticancer Drugs for Cancer Treatment. *Mater. Today* **2014**, 17, 298–306.

18. Pincus, P. Colloid Stabilization with Grafted Polyelectrolytes. *Macromolecules* **1991**, 24, 2912–2919.
19. Ross, R. S.; Pincus, P. The Polyelectrolyte Brush: Poor Solvent. *Macromolecules* **1992**, 25, 2177–2183.
20. Miklavic, S. J.; Marcelja, S. Interaction of Surfaces Carrying Grafted Polyelectrolytes. *J. Phys. Chem.*, **1988**, 92, 6718–6722.
21. Misra, S.; Varanasi, S.; Varanasi, P. P. A Polyelectrolyte Brush Theory. *Macromolecules* **1989**, 22, 4173–4179.
22. Borisov, O. V.; Birshtein, T. M.; Zhulina, E. B. Collapse of Grafted Polyelectrolyte Layer. *J. Phys. II* **1991**, 1, 521–526.
23. Zhulina, E. B.; Rubinstein, M.; Ionic Strength Dependence of Polyelectrolyte Brush Thickness. *Soft Matter* **2012**, 8, 9376–9383.
24. Zhulina, E. B.; Borisov, O. V. Structure and Interaction of Weakly Charged Polyelectrolyte Brushes: Self-Consistent Field Theory. *J. Chem. Phys.* **1997**, 107, 5952–5967.
25. Zhulina, E. B.; Borisov, O. V. Poisson–Boltzmann Theory of pH-Sensitive (Annealing) Polyelectrolyte Brush. *Langmuir* **2011**, 27, 10615–10633.
26. Mei, Y.; Lauterbach, K.; Hoffmann, M.; Borisov, O. V.; Ballauff, M.; Jusufi, A. Collapse of Spherical Polyelectrolyte Brushes in the Presence of Multivalent Counterions. *Phys. Rev. Lett.* **2006**, 97, 158301.
27. Sachar, H. S.; Sivasankar, V. S.; Das, S. Revisiting the Strong Stretching Theory for pH-Responsive Polyelectrolyte Brushes: Effects of Consideration of Excluded Volume

Interactions and an Expanded form of the Mass Action Law. *Soft Matter* **2019**, 15, 559–574.

28. Csajka, F. S.; Seidel, C. Strongly Charged Polyelectrolyte Brushes: A Molecular Dynamics Study. *Macromolecules* **2000**, 33, 2728–2739.
29. He, G. L.; Merlitz, H.; Sommer, J. U. Molecular Dynamics Simulations of Polyelectrolyte Brushes under Poor Solvent Conditions: Origins of Bundle Formation. *J. Chem. Phys.* **2014**, 140, 104911.
30. Sandberg, D. J.; Carrillo, J. M. Y.; Dobrynin, A. V. Molecular Dynamics Simulations of Polyelectrolyte Brushes: From Single Chains to Bundles of Chains. *Langmuir* **2007**, 23, 12716–12728.
31. Desai, P. R.; Sinha, S.; Das, S. Polyelectrolyte Brush Bilayers in Weak Interpenetration Regime: Scaling Theory and Molecular Dynamics Simulations. *Phys. Rev. E* **2018**, 97, 032503.
32. Mei, Y.; Hoffmann, M.; Ballauff, M.; Jusufi, A. Spherical Polyelectrolyte Brushes in the Presence of Multivalent Counterions: The Effect of Fluctuations and Correlations as Determined by Molecular Dynamics Simulations. *Phys. Rev. E* **2008**, 77, 031805.
33. Carrillo, J. M. Y.; Dobrynin, A. V. Morphologies of Planar Polyelectrolyte Brushes in a Poor Solvent: Molecular Dynamics Simulations and Scaling Analysis. *Langmuir* **2009**, 25, 13158–13168.
34. Hehmeyer, O. J.; Stevens, M. J. Molecular Dynamics Simulations of Grafted Polyelectrolytes on Two Apposing Walls. *J. Chem. Phys.* **2005**, 122, 134909.

35. Jackson, N. E.; Brettmann, B. K.; Vishwanath, V.; Tirrell, M.; de Pablo, J. J. Comparing Solvophobic and Multivalent Induced Collapse in Polyelectrolyte Brushes. *ACS Macro Lett.* **2017**, 6, 155–160.

36. Merlitz, H.; Li, C.; Wu, C.; Sommer, J. U. Polyelectrolyte Brushes in External Fields: Molecular Dynamics Simulations and Mean-Field Theory. *Soft Matter* **2015**, 11, 5688–5696.

37. Kumar, N. A.; Seidel, C. Polyelectrolyte Brushes with Added Salt. *Macromolecules* **2005**, 38, 9341–9350.

38. Wittemann, A.; Drechsler, M.; Talmon, Y.; Ballauff, M. High Elongation of Polyelectrolyte Chains in the Osmotic Limit of Spherical Polyelectrolyte Brushes: A Study by Cryogenic Transmission Electron Microscopy. *J. Am. Chem. Soc.* **2005**, 127, 9688–9689.

39. Biesalski, M.; Johannsmann, D.; Rühe, J. Electrolyte-Induced Collapse of a Polyelectrolyte Brush. *J. Chem. Phys.* **2004**, 120, 8807–8814.

40. Balastre, M.; Li, F.; Schorr, P.; Yang, J.; Mays, J. W.; Tirrell, M. V. A Study of Polyelectrolyte Brushes Formed from Adsorption of Amphiphilic Diblock Copolymers Using the Surface Forces Apparatus. *Macromolecules* **2002**, 35, 9480–9486.

41. Yu, J.; Jackson, N. E.; Xu, X.; Morgenstern, Y.; Kaufman, Y.; Ruths, M.; de Pablo, J. J.; Tirrell, M. Multivalent Counterions Diminish the Lubricity of Polyelectrolyte Brushes. *Science* **2018**, 360, 1434–1438.

42. Yu, J.; Jackson, N. E.; Xu, X.; Brettmann, B. K.; Ruths, M.; de Pablo, J. J.; Tirrell, M. Multivalent Ions Induce Lateral Structural Inhomogeneities in Polyelectrolyte Brushes. *Sci. Adv.* **2017**, 3, eaao1497.

43. Yu, J.; Mao, J.; Yuan, G.; Satija, S.; Chen, W.; Tirrell, M. The Effect of Multivalent Counterions to the Structure of Highly Dense Polystyrene Sulfonate Brushes. *Polymer* **2016**, 98, 448–453.
44. Yu, J.; Mao, J.; Yuan, G.; Satija, S.; Jiang, Z.; Chen, W.; Tirrell, M. Structure of Polyelectrolyte Brushes in the Presence of Multivalent Counterions. *Macromolecules* **2016**, 49, 5609–5617.
45. Mahalik, J. P.; Yang, Y.; Deodhar, C.; Ankner, J. F.; Lokitz, B. S.; Kilbey, S. M.; Sumpter, B. G.; Kumar, R. Monomer Volume Fraction Profiles in pH Responsive Planar Polyelectrolyte Brushes. *J. Polym. Sci., Part B: Polym. Phys.* **2016**, 54, 956–964.
46. Farina, R.; Laugel, N.; Pincus, P.; Tirrell, M. Brushes of Strong Polyelectrolytes in Mixed Mono-and Tri-Valent Ionic Media at Fixed Total Ionic Strengths. *Soft Matter* **2013**, 9, 10458–10472.
47. Schneider, C.; Jusufi, A.; Farina, R.; Pincus, P.; Tirrell, M.; Ballauff, M. Stability Behavior of Anionic Spherical Polyelectrolyte Brushes in the Presence of La (III) Counterions. *Phys. Rev. E* **2010**, 82, 011401.
48. Perez Sirkin, Y. A.; Szleifer, I.; Tagliazucchi, M. Voltage-Triggered Structural Switching of Polyelectrolyte-Modified Nanochannels. *Macromolecules* **2020**, 53, 2616–2626.
49. Yameen, B.; Ali, M.; Neumann, R.; Ensinger, W.; Knoll, W.; Azzaroni, O. Single Conical Nanopores Displaying pH-tunable Rectifying Characteristics. Manipulating Ionic Transport with Zwitterionic Polymer Brushes. *J. Am. Chem. Soc.* **2009**, 13, 2070–2071.
50. Ali, M.; Yameen, B.; Cervera, J.; Ramirez, P.; Neumann, R.; Ensinger, W.; Knoll, W.; Azzaroni, O. Layer-By-Layer Assembly of Polyelectrolytes into Ionic Current Rectifying

Solid-State Nanopores: Insights from Theory and Experiment. *J. Am. Chem. Soc.* **2010**, 132, 8338–8348.

51. Sappidi, P.; Natarajan, U. Polyelectrolyte Conformational Transition in Aqueous Solvent Mixture Influenced by Hydrophobic Interactions and Hydrogen Bonding Effects: PAA–Water–Ethanol. *J. Mol. Graph. Model.* **2016**, 64, 60–74.
52. Sulatha, M. S.; Natarajan, U. Origin of the Difference in Structural Behavior of poly (acrylic acid) and poly (methacrylic acid) in Aqueous Solution Discerned by Explicit-Solvent Explicit-ion MD Simulations. *Ind. Eng. Chem.* **2011**, 50, 11785–11796.
53. Sulatha, M. S.; Natarajan, U. Molecular Dynamics Simulations of Adsorption of poly (acrylic acid) and poly (methacrylic acid) on dodecyltrimethylammonium chloride Micelle in Water: Effect of Charge Density. *J. Phys. Chem. B* **2015**, 119, 12526–12539.
54. Ramachandran, S.; Katha, A. R.; Kolake, S. M.; Jung, B.; Han, S. Dynamics of Dilute Solutions of poly (aspartic acid) and its sodium Salt Elucidated from Atomistic Molecular Dynamics Simulations with Explicit Water. *J. Phys. Chem. B* **2013**, 117, 13906–13913.
55. Meneses-Juárez, E.; Márquez-Beltrán, C.; González-Melchor, M. Influence of pH on the Formation of a Polyelectrolyte Complex by Dissipative Particle Dynamics Simulation: From an Extended to a Compact Shape. *Phys. Rev. E* **2019**, 100, 012505.
56. Hao, Q. H.; Liu, L. X.; Xia, G.; Liu, L. Y.; Miao, B. The Effects of Grafting Density and Charge Fraction on the Properties of Ring Polyelectrolyte Brushes: A Molecular Dynamics Simulation Study. *Colloid Polym. Sci.* **2020**, 298, 21–33.
57. Santos, D. E.; Li, D.; Ramstedt, M.; Gautrot, J. E.; Soares, T. A. Conformational Dynamics and Responsiveness of Weak and Strong Polyelectrolyte Brushes: Atomistic

Simulations of Poly (dimethyl aminoethyl methacrylate) and Poly (2-(methacryloyloxy) ethyl trimethylammonium chloride). *Langmuir* **2019**, 35, 5037–5049.

58. An, S. W.; Thirtle, P. N.; Thomas, R. K.; Baines, F. L.; Billingham, N. C.; Armes, S. P.; Penfold, J. Structure of a Diblock Copolymer Adsorbed at the Hydrophobic Solid/Aqueous Interface: Effects of Charge Density on a Weak Polyelectrolyte Brush. *Macromolecules* **1999**, 32, 2731–2738.
59. Topham, P. D.; Glidle, A.; Toolan, D. T.; Weir, M. P.; Skoda, M. W.; Barker, R.; Howse, J. R. The Relationship between Charge Density and Polyelectrolyte Brush Profile using Simultaneous Neutron Reflectivity and In Situ Attenuated Total Internal Reflection FTIR. *Langmuir* **2013**, 29, 6068–6076.
60. Sachar, H. S.; Pial, T. H.; Desai, P. R.; Etha, S. A.; Wang, Y.; Chung, P. W.; Das, S. Densely Grafted Polyelectrolyte Brushes Trigger "Water-in-Salt"-like Scenarios and Ultraconfinement Effect. *Matter* **2020**.
61. Berendsen, H. J. C.; Grigera, J. R.; Straatsma, T. P. The Missing Term in Effective Pair Potentials. *J. Phys. Chem.* **1987**, 91, 6269–6271.
62. Duboué-Dijon, E.; Laage, D. Characterization of the Local Structure in Liquid Water by Various Order Parameters. *J. Phys. Chem. B* **2015***,* 119, 8406–8418.
63. Plimpton, S. Fast Parallel Algorithms for Short-range Molecular Dynamics. *J. Comput. Phys*. **1995**, 117, 1–19.
64. Jorgensen, W. L.; Maxwell, D. S.; Tirado-Rives, J. Development and Testing of the OPLS All-atom Force Field on Conformational Energetics and Properties of Organic Liquids. *J. Am. Chem. Soc*. **1996**, 118, 11225–11236.

65. Joung, I. S.; Cheatham III, T. E. Determination of Alkali and Halide Monovalent Ion Parameters for Use in Explicitly Solvated Biomolecular Simulations. *J. Phys. Chem. B* **2008**, 112, 9020–9041.

66. Hockney, R. W.; Eastwood, J. W. *Computer Simulations Using Particles*; McGraw-Hill International Book Co, New York, 1981.

67. Ryckaert, J.-P.; Ciccotti, G.; Berendsen, H. J. Numerical Integration of the Cartesian Equation of Motion of a System with Constraints: Molecular Dynamics of n-Alkanes. *J. Comput. Phys.* **1977***,* 23, 327–341.

68. Hoover, W. G. Canonical Dynamics: Equilibrium Phase-Space Distributions. *Phys. Rev. A* **1985**, 31, 1695–1697.

69. Nosé, S. A Unified Formulation of the Constant Temperature Molecular Dynamics Methods. *J. Chem. Phys*. **1984**, 81, 511–519.

70. Schneider, T.; Stoll, E. Molecular-Dynamics Study of a Three-Dimensional One-Component Model for Distortive Phase Transitions. *Phys. Rev. B* **1987***,* 17, 1302–1322.

71. Stukowski, A. Visualization and Analysis of Atomistic Simulation Data with OVITO–the Open Visualization Tool. *Model. Simul. Mater. Sci. Eng.* **2010**, 18, 015012.

72. Swift, T.; Swanson, L.; Geoghegan, M.; Rimmer, S. The pH-responsive Behaviour of poly (acrylic acid) in Aqueous Solution is Dependent on Molar Mass. *Soft Matter* **2016**, 12, 2542–2549.

73. Ahrens, H.; Förster, S.; Helm, C. A.; Kumar, N. A.; Naji, A.; Netz, R. R.; Seidel, C. Nonlinear Osmotic Brush Regime: Experiments, Simulations and Scaling Theory. *J. Phys. Chem. B* **2004**, 108, 16870–16876.

74. Nair, A. Molecular Dynamics Simulations of Polyelectrolyte Brushes. Ph.D. Dissertation, King Abdullah University of Science and Technology, Saudi Arabia, 2006.

75. Naji, A.; Netz, R. R.; Seidel, C. Non-Linear Osmotic Brush Regime: Simulations and Mean-Field Theory. *Eur. Phys. J. E* **2003**, 12, 223–237.

76. Elton, D. C. Understanding the Dielectric Properties of Water. Ph.D. Dissertation, The Graduate School, Stony Brook University: Stony Brook, NY, 2016.

77. Guardia, E.; Martí, J.; García-Tarrés, L.; Laria, D. A Molecular Dynamics Simulation Study of Hydrogen Bonding in Aqueous Ionic Solutions. *J. Mol. Liq.* **2005**, 117, 63−67.

78. Luzar, A.; Chandler, D. Structure and Hydrogen Bond Dynamics of Water–Dimethyl Sulfoxide Mixtures by Computer Simulations. *J. Chem. Phys.* **1993**, 98, 8160−8173.

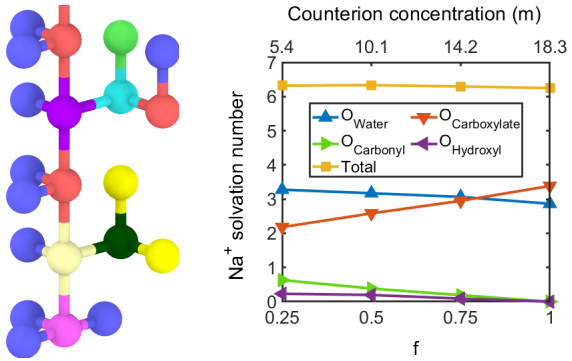

All-atom Molecular Dynamics simulations are used to probe the effects of charge density on the microstructure of polyacrylic acid brushes.